Photoinduced Electron Transfer in Multiporphyrinic Interlocked Structures: The Effect of Copper(I) Coordination in the Central Site

Lucia Flamigni,*[a] Anna Maria Talarico,[a] Jean-Claude Chambron,[b, c] Valérie Heitz,[b] Myriam Linke,[b, d] Norifumi Fujita,[b, e] and Jean-Pierre Sauvage*[b]

Abstract: Photoinduced processes have been determined in a [2]catenane containing a zinc(II) porphyrin, a gold(III) porphyrin, and two free phenanthroline binding sites, **Zn–Au$^+$**, and in the corresponding copper(I) phenanthroline complex, **Zn–Cu$^+$–Au$^+$**. In acetonitrile solution **Zn–Au$^+$** is present in two different conformations: an extended one, L, which accounts for 40% of the total, and a compact one, S. In the L conformation, the electron transfer from the excited state of the Zn porphyrin to the gold–porphyrin unit ($k = 1.3 \times 10^9\ s^{-1}$) is followed by a slow recombination ($k = 8.3 \times 10^7\ s^{-1}$) to the ground state. The processes in the S conformation cannot be clearly resolved but a charge-separated (CS) state is rapidly formed and decays with a lifetime on the order of fifty picoseconds. In the catenate **Zn–Cu$^+$–Au$^+$**, the zinc–porphyrin excited state initially transfers energy to the Cu^I–phenantholine unit, producing a metal-to-ligand charge-transfer (MLCT) excited state localized on the copper complex with a rate $k = 1.4 \times 10^9\ s^{-1}$. From this excited state the transfer of an electron to the gold–porphyrin unit takes place, producing the CS state **Zn–Cu^{2+}–Au$^{\cdot}$**, which decays with a lifetime of 10 ns. The results are discussed in comparison with the closely related [2]rotaxane, in which a further charge shift from the copper center to the zinc–porphyrin unit leads to the fully CS state. Even in the absence of such full charge separation, it is shown that the lifetimes of the CS states are increased by a factor of about 2–2.5 over those of the corresponding rotaxanes.

Keywords: catenanes · charge separation · electron transfer · photochemistry · porphyrinoids

Introduction

Porphyrinic chromophores are among the most widely used components in the preparation of synthetic arrays able to undergo photoinduced energy and electron transfer processes.[1] Because of their remarkable spectroscopic and electrochemical properties,[2] which can be finely tuned by substitution or metalation, such chromophores have proven to be versatile components able to act as energy donors or acceptors as well as electron donors and acceptors in a variety of multicomponent arrays designed to achieve useful functions triggered by light. In general, Zn^{II}–porphyrin components (energy of the lowest singlet excited state is about 2.1 eV and the oxidation potential versus SCE is on the order of 0.7 V) have often been used as energy and electron donors. Free base porphyrins have been mostly employed as energy acceptors or electron donors (lowest singlet excited state about 1.9 eV, oxidation potential 0.9 V versus SCE). Au^{III}–porphyrins have been utilized by several groups as electron acceptors (reduction potential versus SCE on the order of −0.6 V).[3–5] The incorporation of porphyrins into photoactive multicomponent assemblies as covalently linked arrays[3] or architectures that assemble upon weak interactions in solution[4] has been widespread over the last decade,

[a] Dr. L. Flamigni, Dr. A. M. Talarico
Istituto per la Sintesi Organica e Fotoreattivita' (ISOF), CNR
Via P. Gobetti 101, 40129 Bologna (Italy)
Fax: (+39) 051-639-9844
E-mail: flamigni@isof.cnr.it

[b] Dr. J.-C. Chambron, Dr. V. Heitz, Dr. M. Linke, Dr. N. Fujita, Dr. J.-P. Sauvage
Laboratoire de Chimie Organo-Minérale, UMR 7513 CNRS
Université Louis Pasteur, Institut Le Bel
4 rue Blaise Pascal, 67070 Strasbourg (France)
Fax: (+33) 03-902-41368
E-mail: sauvage@chimie.u-strasbg.fr

[c] Dr. J.-C. Chambron
Current address: LIMSAG (UMR 5633 du CNRS)
Université de Bourgogne, Faculté des Sciences "Gabriel"
6 boulevard Gabriel, 21000 Dijon (France)

[d] Dr. M. Linke
Current address: Forschungszentrum Karlsruhe
Institute for Nanotechnology
Postfach 3640, 76021 Karlsruhe (Germany)

[e] Dr. N. Fujita
Current address: Department of Chemistry and Biochemistry
Graduate School of Engineering, Kyushu University
6-10-1 Hakazaki, Higashi-ku, Fukuoka 812-8581 (Japan)

 DOI: 10.1002/chem.200305655

whereas examples of photoactive, porphyrinic, interlocked structures are rare.[5] The reason for this must mainly be ascribed to the limited availability of interlocked structures in comparison with other types of arrays. Only recently, thanks to synthetic strategies relying on several types of "template effect",[6] have catenanes and rotaxanes become accessible chemical products, having been mostly chemical curiosities for decades.[7] Inclusion of porphyrinic chromophores in these structures offers the opportunity to test electronic interactions between entities that are not chemically connected through the study of photoinduced energy- and electron-transfer processes between components. This is, per se, an important advancement of knowledge related to the fields of physics, chemistry, and biology. Furthermore, this type of architecture, characterized by mechanical linkages that force the components to assume relatively fixed positions without connecting them by direct chemical bonds, more closely mimics the organization of the tetrapyrrolic pigments in the complexes used for light energy collection (antennas) and charge separation (reaction centers) in natural photosynthetic systems.[8] In the latter case the porphyrinic chromophores are embedded in a protein scaffold, which provides both a precise arrangement in space and the necessary electronic coupling. Therefore, in the frame of a biomimetic approach to the conversion of light energy into chemical energy, this type of structure offers an important opportunity to study the parameters affecting the efficiency of the process.

Our groups have previously reported on photoinduced electron transfer in a [2]rotaxane $\mathbf{Zn_2–Au^+}$, a gold–porphyrin-containing macrocycle threaded onto a dumbbell with two zinc porphyrins as stoppers, and the corresponding metalated $\mathbf{Zn_2–Cu^+–Au^+}$, obtained by binding Cu^I to the phenanthroline components of the macrocycle and the dumbbell (Figure 1a).[5e] In the extended conformation of the free rotaxane $\mathbf{Zn_2–Au^+}$, which accounts for 30% of the total conformations, electron transfer from the lowest excited state of the zinc–porphyrin unit to the gold–porphyrin acceptor occurred, yielding a charge-separated state $\mathbf{Zn_2^{+\cdot}–Au^{\cdot}}$, which is characterized by an oxidized zinc porphyrin and a reduced gold–porphyrin radical and has a lifetime of 5.5 ns. In the copper-containing array, $\mathbf{Zn_2–Cu^+–Au^+}$, the excited state of the zinc porphyrin was postulated to transfer energy to the copper complex unit first, yielding the excited state $\mathbf{Zn_2–{}^*Cu^+–Au^+}$, which in turn could transfer an electron to the gold porphyrin to yield the charge-separated state $\mathbf{Zn_2–Cu^{2+}–Au^{\cdot}}$, characterized by a Cu^{II} unit and a reduced gold porphyrin. Subsequent charge shift from the zinc–porphyrin unit, thermodynamically allowed because of the unusually high oxidation potential of the bis(zinc–porphyrin)-substituted copper complex (ca. 1 V versus SCE), yields the charge-separated state $\mathbf{Zn_2^{+\cdot}–Cu^+–Au^{\cdot}}$, with oxidized zinc–porphyrin termini and a reduced gold–porphyrin end group characterized by a lifetime of 5 ns (Figure 1a).[5e]

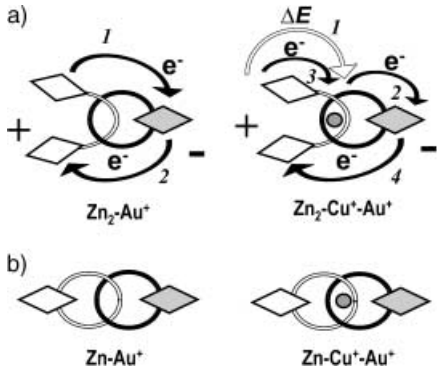

Figure 1. Schematic representation of a) photoinduced processes in the [2]rotaxane; b) structure of the [2]catenanes. Both energy transfer and electron transfer between porphyrinic units (rhombs) are reported, the sequence of elementary steps is represented by arabic numbers. Copper(I) atoms appear as gray circles.

In this report we examine the photoinduced processes in the related catenanes[9] $\mathbf{Zn–Cu^+–Au^+}$ and $\mathbf{Zn–Au^+}$ (Figure 1b, Scheme 1). We intend to assess 1) the effect, on the electron-transfer rates, of increasing the center-to-center distance between the electron donor and the acceptor in the free catenane $\mathbf{Zn–Au^+}$ (2.6 nm) compared with the case of the rotaxane $\mathbf{Zn_2–Au^+}$ (1.9 nm), and in the copper-containing structure $\mathbf{Zn–Cu^+–Au^+}$ (2.6 nm) compared with $\mathbf{Zn_2–Cu^+–Au^+}$ (1.9 nm); and 2) to test the effect of decreasing the driving force for the postulated charge-shift reaction that leads to the final charge-separated state in $\mathbf{Zn–Cu^+–Au^+}$ with respect to the $\mathbf{Zn_2–Cu^+–Au^+}$ case (see above).

Results and Discussion

Electrochemistry: The electrochemical data of the reference compounds $\mathbf{Cu^+}$, **Au**, and **Zn**, as well as those of the [2]catenates $\mathbf{Zn–Cu^+}$ and $\mathbf{Zn–Cu^+–Au^+}$ are gathered in Table 1.

Table 1. Electrochemical data for the catenanes: V versus Fc^+/Fc [mV, ΔE_p]; 0.1 M tetrabutylammoniumhexafluorophosphate in butyronitrile.

	Cu^{2+}/Cu^+	$Zn^{+\cdot}/Zn$	$Au^+/Au^{\cdot}$	$Zn/Zn^{-\cdot}$
$\mathbf{Cu^+}$	+0.14 (70)			
$\mathbf{Au^+}$			−1.03 (50)	
Zn		+0.28 (70)		−1.88 (70)
$\mathbf{Zn–Cu^+}$	+0.14 (65)	+0.25 (70)		−1.86 (70)
$\mathbf{Zn–Cu^+–Au^+}$	+0.29 (80)	+0.29 (80)	−1.02 (60)	−1.85 (65)

The redox potentials of the [2]catenane $\mathbf{Zn–Au^+}$ are assumed to be identical to those of its separated components, macrocycles **Zn** and $\mathbf{Au^+}$, since there is only very weak coupling between the porphyrins, as evidenced in the absorption spectra (see below), and no stacking between the porphyrins, as evidenced by the NMR studies.[9] The reduction of the gold(III) porphyrin and the oxidation of the zinc(II) porphyrin in $\mathbf{Zn–Cu^+}$ and $\mathbf{Zn–Cu^+–Au^+}$ occur nearly at the same potential as for the models **Zn** or $\mathbf{Au^+}$. In contrast, the oxidation potential of copper(I) varies depending on stereoelectronic factors, as already mentioned in the rotaxane series.[5e] In $\mathbf{Zn–Cu^+}$, the Cu^I complex subunit is oxidized at +0.14 V versus Fc^+/Fc, as in $\mathbf{Cu^+}$, but in $\mathbf{Zn–Cu^+–Au^+}$, the same oxidation step is found at +0.29 V versus Fc^+/Fc. The 150 mV anodic shift is attributed to an increase of positive

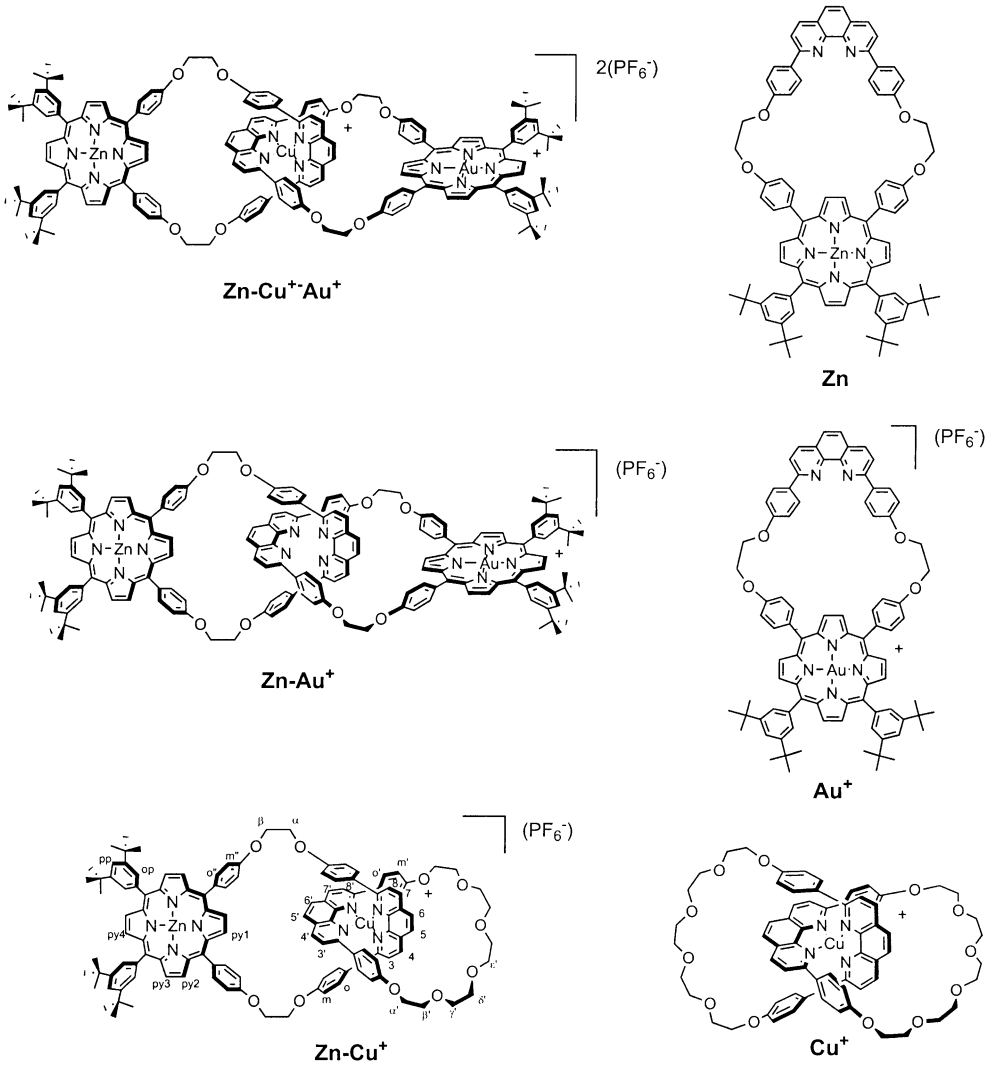

Scheme 1. [2]catenanes and related models.

charge (presence of cationic gold(III) porphyrin) in [2]catenate **Zn–Cu$^+$–Au$^+$** as compared with **Zn–Cu$^+$**. As a result, the zinc porphyrin and the Cu^I complex subunits in **Zn–Cu$^+$–Au$^+$** have identical oxidation potentials (+0.29 V versus Fc^+/Fc) and there is no driving force for the Cu^{II} state to oxidize the zinc–porphyrin subunit in this [2]catenate.

Ground state absorption: The chemical structure of the models **Zn**, **Au$^+$**, and **Cu$^+$** are collected in Scheme 1 together with those of the catenanes **Zn–Cu$^+$**, **Zn–Au$^+$**, and **Zn–Cu$^+$–Au$^+$**. The macrocycles **Zn** and **Au$^+$** better represent the units in the arrays compared with the simple Zn^{II} and Au^{III} 5,10,15,20-tetrakis(3′,5′-di-*tert*-butylphenyl)porphyrins. The absorption spectra of the catenanes **Zn–Cu$^+$**, **Zn–Cu$^+$–Au$^+$**, and **Zn–Au$^+$**, reported in Figure 2 with the absorption spectra of the model units, closely match the superposition of the separate components, with only a very slight broadening of the bands and decrease of the molar absorption coefficients with respect to the sum of the components. This phenomenon, more evident in **Zn–Au$^+$**, is assigned to some interaction between the units owing to the presence of a conformation characterized by a close approach of the por-

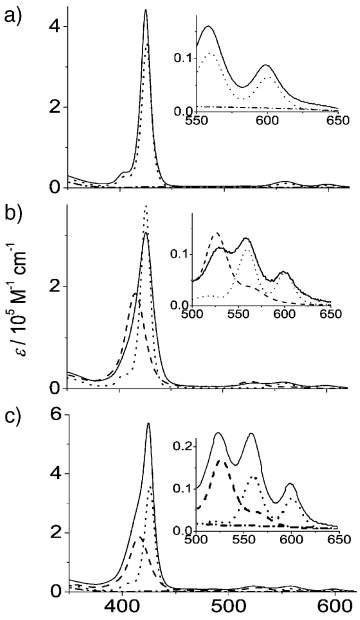

Figure 2. Absorption spectra, acetonitrile solutions, 298 K of: a) **Zn–Cu$^+$** (——), **Zn** (•••••) and **Cu$^+$** (–•–•); b) **Zn–Au$^+$**(——), **Zn** (•••••), **Au$^+$** (– – –); c) **Zn–Cu$^+$–Au$^+$** (——), **Zn** (•••••), **Au$^+$** (– – –) and **Cu$^+$** (–•–•).

phyrinic units in the free catenane (see below). Nonetheless, both spectroscopic and electrochemical determinations indicate that the interactions are weak in all the arrays.

Luminescence: The luminescence properties of the models in acetonitrile solutions, determined at 298 K and 77 K, are collected in Table 2. At 298 K, excitation of the Zn porphyrin units in the catenanes at 558 nm resulted in the quenching, to different extents, of the zinc-porphyrin-based luminescence in all the catenanes. In Figure 3, the emission spectra of the catenanes compared with those of the model **Zn** are shown, and the calculated emission quantum yields ϕ_f are reported in Table 2. These make it appear that the Zn porphyrin luminescence in **Zn–Au$^+$** is lower than in **Zn–Cu$^+$**, which is in turn lower than in **Zn–Cu$^+$–Au$^+$**.

Table 2. Luminescence properties at 298 K[a] and 77 K[b], air-equilibrated solutions.

		298 K				77 K	
		λ_{max} [nm]	τ [ns]	ϕ_f	k_r [s^{-1}]	λ_{max} [nm]	E [eV]
Zn[c]	^{1}Zn	607	2.1	0.070	3.3×10^7	608	2.04
	^{3}Zn					802	1.55
Au$^+$	^{3}Au$^+$					718	1.73
Cu$^+$[d]	*Cu$^+$	710	85	0.0003	3.5×10^3	700	1.77
Zn–Cu$^+$	^{1}Zn–Cu$^+$	603	0.320	0.01	3.1×10^7	606	2.05
	^{3}Zn–Cu$^+$					800	1.55
Zn–Au$^+$	^{1}Zn–Au$^+$	606	0.570	0.008	1.4×10^7[e]	606	2.05
	^{3}Zn–Au$^+$					802	1.55
	Zn–^{3}Au$^+$					716	1.73
Zn–Cu$^+$–Au$^+$	^{1}Zn–Cu$^+$–Au$^+$	606	0.540	0.021	3.3×10^7	604	2.05
	^{3}Zn–Cu$^+$–Au$^+$					796	1.56
	Zn–Cu$^+$–^{3}Au$^+$					716	1.73

[a] In acetonitrile, except otherwise specified. [b] Butyronitrile. [c] Acetonitrile/butyronitrile (1/1). [d] From reference [5e]. [e] Apparent radiative rate. This value is due to the presence of different conformations (see text).

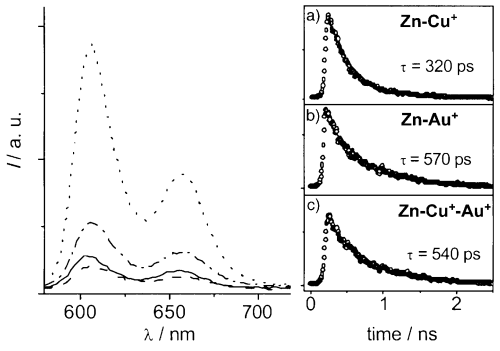

Figure 3. Fluorescence spectra of **Zn** (•••••), **Zn–Cu$^+$** (——), **Zn–Au$^+$** (– – –), and **Zn–Cu$^+$–Au$^+$** (–•–•) in acetonitrile solutions at 298 K upon excitation at 558 nm, with the absorption adjusted to have the same number of photons absorbed by the Zn porphyrin moiety. Luminescence decays upon excitation with a 35 ps laser pulse at 532 nm are reported on the right side.

The luminescence decays of the zinc porphyrin in the catenanes (Figure 3) are satisfactorily fitted by a single exponential corresponding to a lifetime of 320 ps for **Zn–Cu$^+$**, 570 ps for **Zn–Au$^+$**, and 540 ps for **Zn–Cu$^+$–Au$^+$** (Table 2). The trend of the lifetimes does not parallel the luminescence yield for all compounds and this is reflected by the calculated radiative rate constants ($k_r = \phi_f/\tau$) reported in Table 2. Whereas the radiative rate constants for the catenanes **Zn–Cu$^+$** and **Zn–Cu$^+$–Au$^+$** are in agreement with those of the related models, in the case of **Zn–Au$^+$** it is less than 50% that of the model **Zn**. This apparent discrepancy can be explained on the basis of the existence of two different, extreme conformations in the flexible **Zn–Au$^+$**: an extended one, with the gold and the zinc–porphyrin nuclei at a large distance from one another (long conformation, L) and a more compact conformation, where the porphyrinic components are in close proximity (short conformation, S), Scheme 2. The luminescence quenching in the L conformation is expected to be slower than in the S conformation, in which the electron donor and acceptor can react immediately (static quenching). Whereas the quenching due to both conformations can be detected in the steady-state luminescence experiments, in which the emission is integrated over the time, only the quenched lifetimes longer than our time resolution (20 ps) can be measured in time-resolved experiments. Since the time-resolved luminescence of **Zn–Au$^+$** indicates a single lifetime of 570 ps, we have to assume that the quenching process for the S conformation is faster than

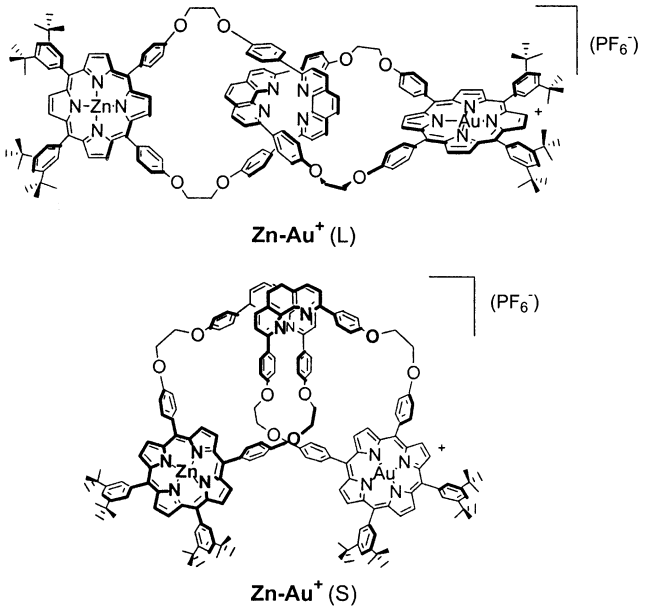

Scheme 2. Extended or long conformation (L) and compact or short conformation (S) of **Zn–Au$^+$**.

the 20 ps resolution. Assuming k_r is constant over the series, $(3.4 \pm 0.4) \times 10^7\ s^{-1}$, the fractions of the different conformation can be calculated on the basis of the following equation: $\phi_f = f_S \tau_S k_r + f_L \tau_L k_r$, in which f_L and τ_L are the fraction and the lifetime of the L conformation and f_S and τ_S are the fraction and the lifetime of the S conformation. By inserting the experimental value for ϕ_f (0.008) and the lifetime values for the S conformation, $0 \leq \tau_S \leq 20$ ps, and for the L conformation, 570 ps into this equation, fractions of about 40% and 60% are derived for the L and S components respectively.

Energy level schemes: On the basis of the electrochemical data (Table 1) and the spectroscopic data, which allow us to derive the energy levels of the excited states (Table 2), it is possible to derive the energy level schemes for the catenanes, which are reported in Figure 4. It should be taken into account that the **Au$^+$** unit has a singlet excited state not reported in the energy level scheme, with an energy of about 2.2 eV and a lifetime of 240 fs.[10] Given the extremely short lifetime of this state, the gold–porphyrin singlet is not relevant to the dynamics of photoinduced processes and is therefore not taken into account here.

For **Zn–Cu$^+$** (Figure 4a), the most probable process for quenching the singlet excited state localized on porphyrin, **^{1}Zn–Cu$^+$**, appears to be an energy transfer to the excited state localized on the metal complex, **Zn–*Cu$^+$**. An alternative path, involving reductive quenching of the zinc–porphyrin excited state by the ground-state copper complex, displays too low a driving force to compete, this view being adequately supported in the following section. It should be recalled that the above energy-transfer process is possible because the lowest excited state localized on the copper complex and indicated as **Zn–*Cu$^+$** is an equilibrium mixture of a metal-to-ligand charge-transfer singlet excited state (^{1}MLCT) and the corresponding triplet (^{3}MLCT).[11]

In contrast, for **Zn–Au$^+$** (Figure 4b) the only possible process for quenching the zinc–porphyrin luminescence is an electron transfer to the gold–porphyrin unit to yield a charge-separated state (CS) **Zn$^{+\bullet}$–Au$^{\bullet}$**. Energy transfer from the zinc–porphyrin excited singlet to the gold–porphyrin excited triplet would be forbidden by spin selection rules.

For **Zn–Cu$^+$–Au$^+$** (Figure 4c), starting from the excited porphyrin unit **^{1}Zn–Cu$^+$–Au$^+$**, both the following processes are in principle thermodynamically allowed, 1) electron transfer yielding the CS state **Zn$^{+\bullet}$–Cu$^+$–Au$^{\bullet}$** with a hole on the zinc porphyrin and an extra electron on the gold porphyrin, and 2) energy transfer to **Zn–*Cu$^+$–Au$^+$**. Kinetic parameters will cause one to prevail over the other, as detailed below.

Transient absorption spectroscopy: The interpretation of the transient absorption spectra of these catenanes is not simple; at 532 nm (excitation wavelength of Nd-YAG laser) most photons are absorbed by the Au–porphyrin component (ca. 80% of photons are absorbed by the Au–porphyrin component and ca. 20% by the Zn–porphyrin unit for both catenanes). Therefore the prevalent excited state, formed in less than 1 ps from the ^{1}Au$^+$,[10] is ^{3}Au$^+$, which displays a strong absorption band in a spectral region of interest (550 nm–750 nm) and decays with a lifetime of 1.5 ns, overshadowing most of the faster phenomena.

Zn–Cu$^+$: Figure 5 depicts the spectra recorded for **Zn–Cu$^+$** at the end of a 35 ps pulse and 3 ns after the pulse. The end-of-pulse spectrum is characterized by an intense absorbance with a maximum around 460 nm. The stimulated emission bands are around 605 nm and 660 nm, typical of the por-

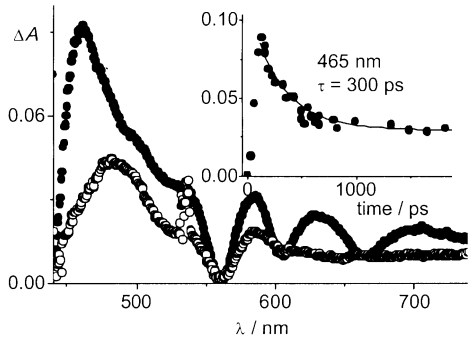

Figure 5. Differential transient absorption spectra registered after a 35 ps laser pulse (532 nm, 2.5 mJ) in an acetonitrile solution of **Zn–Cu$^+$**. End-of-pulse spectrum (●) and after 3 ns (○); the transient absorption decay at 465 nm and relative fitting are reported in the inset.

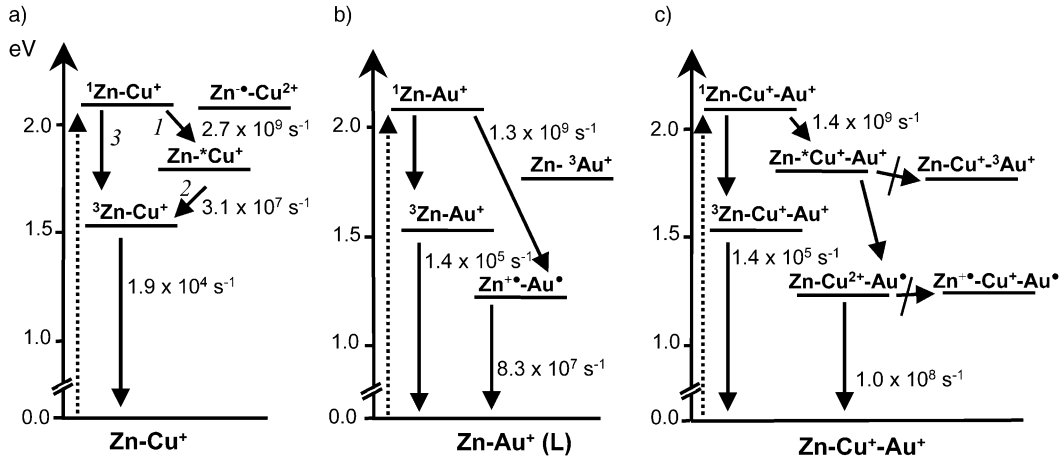

Figure 4. Schematic energy level diagrams.

phyrin singlet, and overlay the bleaching of the ground state absorption because of the Q bands at 560 nm and 600 nm. The time evolution measured at 465 nm can be fitted by a mono-exponential decay with a lifetime of 300 ps, (Figure 5, inset) in good agreement with the 320 ps fluorescence decay. The **^{1}Zn–Cu$^+$** decay is assigned to energy transfer to the copper-phenanthroline unit (Figure 4 a), which leaves an absorption spectrum at 3 ns characterized by a band at 480 nm, typical of the triplet spectrum of the porphyrin, but with a much lower absorbance than in the model porphyrin **Zn**. This can be understood by considering that the product of the energy-transfer process, **Zn–*Cu$^+$**, has a considerably lower absorbance than both **^{1}Zn–Cu$^+$** and **^{3}Zn–Cu$^+$**.[12,13] The spectroscopic evolution at longer times can be studied by means of a flash-photolysis apparatus with nanosecond resolution. The spectra of the catenane **Zn–Cu$^+$**, measured at 30 and 60 ns after an 18 ns laser pulse at 532 nm in an oxygen-free acetonitrile solution, are shown in Figure 6. A

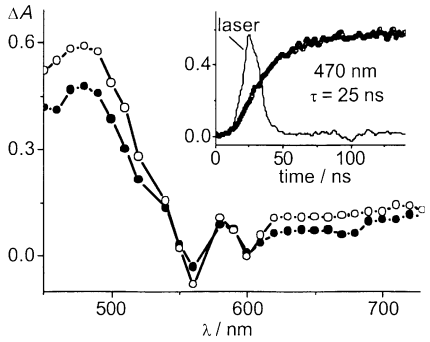

Figure 6. Transient absorption difference detected in air-free acetonitrile solution of **Zn–Cu$^+$** measured at 30 ns (●) and 60 ns (○) after a 18 ns laser pulse (532 nm, 13 mJ). In the inset the rise detected at 470 nm and the fitting is reported with the instrumental profile.

rise in the spectra can be registered immediately after the end of the pulse, which can be fitted by a mono-exponential growth with a lifetime of 25 ns, assigned to the formation of **^{3}Zn–Cu** from the **Zn-*Cu** (Figure 6 inset). The increase in absorbance over the whole spectral region is due to the fact that the molar absorption coefficient of the porphyrin triplet is considerably higher than the one of the excited state localized on the MLCT state of the copper complex at any wavelength.[12,13] The yield of the porphyrin triplet in the array, **^{3}Zn–Cu$^+$**, measured in air-purged solutions at 500 ns delay, was identical to the triplet yield of the model **Zn** (Table 3). This result is in agreement with the mechanism outlined in Figure 4a, for which the triplet yield ϕ_T can be calculated from Equation (1), in which $\eta_{Zn-*Cu+}$ indicates the efficiency of the formation of **Zn–*Cu$^+$** from **^{1}Zn–Cu$^+$**, $\eta_{^3Zn-Cu+}$ is the efficiency of the formation of **^{3}Zn–Cu$^+$** from the state **Zn–*Cu$^+$**, and η_{isc} is the efficiency of formation of **^{3}Zn–Cu$^+$** from the singlet excited state **^{1}Zn–Cu$^+$**.

$$\phi_T = (\eta_{Zn-*Cu^+})(\eta_{^3Zn-Cu^+}) + \eta_{isc} \quad (1)$$

The efficiencies of the elementary steps contributing to the formation of **^{3}Zn–Cu$^+$** (Figure 4a) can be derived from

Table 3. Transient absorbance data, air-free acetonitrile at 298 K.

	State	τ/ns	ϕ_T[a]
Zn[b]	^{1}Zn	2.1	
	^{3}Zn	1.25×10^5	0.79
Au$^+$	^{3}Au$^+$	1.5	
Cu$^+$	*Cu$^+$	110	
Zn–Cu$^+$	^{1}Zn–Cu$^+$	0.300	
	^{3}Zn–Cu$^+$	5.2×10^4	0.79
	Zn–*Cu$^+$	25	
Zn–Au$^+$	^{1}Zn–Au$^+$	0.430[c]	
	^{3}Zn–Au$^+$	6.7×10^3	0.10
	Zn–^{3}Au$^+$	1.5	0.40
	Zn$^{+\cdot}$–Au$^{\cdot}$	12	
Zn–Cu$^+$–Au$^+$	^{1}Zn–Cu$^+$–Au$^+$	0.550	
	^{3}Zn–Cu$^+$–Au$^+$	7.2×10^3	0.39
	Zn–Cu$^+$–^{3}Au$^+$	1.5	1.0
	Zn–Cu^{2+}–Au$^{\cdot}$	10	

[a] Triplet formation quantum yields. [b] acetonitrile/butyronitrile (1:1). [c] Contaminated by the presence of a fast decay, an analysis taking this into account yields a lifetime of 570 ± 50 ps (see text).

the lifetime of the state (τ_i) and the rate of the step (k_i) according to Equation (2).

$$\phi_T = (k_1\tau_{^1Zn-Cu^+})(k_2\tau_{Zn-*Cu^+}) + \phi_{T0}\tau_{^1Zn-Cu^+}/\tau_0 \quad (2)$$

From the lifetime and triplet yield of the model **Zn**, τ_0, and ϕ_{T0}, which can be found with the other parameters in Figure 4 and Table 2, a ϕ_T of 0.77 is derived. This is in perfect agreement with the experimentally determined ϕ_T = 0.79 reported in Table 3. The lifetime of the zinc–porphyrin triplet was determined in conditions of low laser energy to prevent triplet-triplet annihilation phenomena and was measured to be 52 μs.

Zn–Au$^+$: The transient absorption spectra obtained at the end of a 35 ps laser pulse for **Zn–Au$^+$** and the related models **Zn** and **Au$^+$** are shown in Figure 7. The end-of-pulse spectrum of **Zn–Au$^+$** shows the typical absorption bands of **^{1}Zn** (λ_{max} = 460 nm) and **^{3}Au$^+$** (λ_{max} = 630 nm). In addition, some higher absorbance around 670 nm, a wavelength typi-

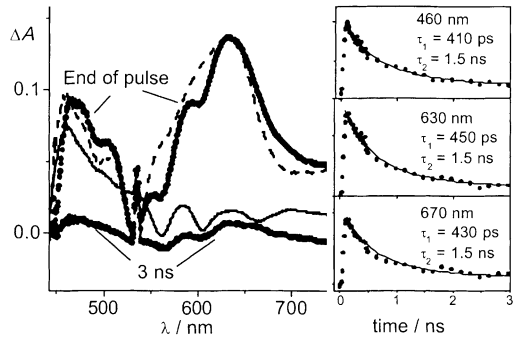

Figure 7. Transient absorption difference detected at the end of a 35 ps laser pulse (532 nm, 2.5 mJ) for acetonitrile solutions of: **Au$^+$** (– – –), **Zn** (——), and **Zn–Au$^+$** (●); differential transient absorbance measured at 3 ns after laser pulse is also reported for **Zn–Au$^+$**. The model absorbance was adjusted to have the same number of photons absorbed by the unit in the array. On the right side are decays and fittings for an acetonitrile solution of **Zn–Au$^+$** at selected wavelengths.

cal of the zinc–porphyrin cation,[14] is evident. The presence of this band at the end of the pulse, before the luminescence of the donor in the L conformation of the catenane starts to decay ($\tau = 570$ ps, Table 2), indicates that this CS state originates from the S conformation. In this conformation, the electron transfer reaction from the zinc–porphyrin donor to the gold–porphyrin acceptor was found to be too fast to be detected with a resolution of 20 ps in the luminescence experiments (see above). The spectrum decays within the time window of the experiments and the absorption changes at the three more representatives wavelengths, 460 nm (^{1}**Zn**), 630 nm (^{3}**Au$^+$**), and 670 nm (**Zn$^+$**), are reported in Figure 7. They show that the decay can be fitted by two exponentials with a nonzero infinite absorbance. The shorter lifetime is around 430 ps (remarkably shorter than the luminescence decay of the zinc-porphyrin luminescence, which is 570 ps) whereas the longer lifetime is 1.5 ns, coincident with the decay of ^{3}**Au$^+$**. It is therefore assigned to **Zn–^{3}Au$^+$**, which is formed by direct excitation of the gold–porphyrin moiety in the catenane. We assign the apparent shortening of the excited ^{1}**Zn–Au$^+$** with respect to the luminescence lifetime decay $\tau = 570$ ps, to overlap with a faster process, which we identify with the decay of the **Zn$^{+\cdot}$–Au$^{\cdot}$** CS state formed in the S conformation. In fact, the decay could be satisfactorily fitted with a three-exponential decay with the same lifetime at the different wavelengths, $\tau_1 = 50 \pm 20$ ps, $\tau_2 = 570 \pm 30$ ps, and $\tau_3 = 1.5 \pm 0.1$ ns, from which a lifetime of about 50 ps for the charge recombination of the S conformation can be derived. As far as the CS state of the extended conformation L is concerned, its formation should have a rate of 570 ps, as derived from the luminescence decay. However, its observation by spectroscopic means is precluded by the absorbance of the **Zn–^{3}Au$^+$**, which displays a strong band in the same spectral region. The yield of the gold–porphyrin-localized triplet **Zn–^{3}Au$^+$** is 0.4 relative to a yield of 1 for the model **Au$^+$**. This indicates that only the L conformation in **Zn–Au$^+$** yields a detectable triplet. In the S conformation **Zn–^{3}Au$^+$** reacts faster than our resolution, very likely by an electron transfer reaction, as reported for similar systems.[5f] At any rate, the spectrum recorded 3 ns after the laser pulse in **Zn–Au$^+$** solutions shows the presence of some absorbance around 670 nm (Figure 7), which can be better investigated by nanosecond flash photolysis. In this experiment, the spectrum obtained in air-free acetonitrile solutions of **Zn–Au$^+$** at the end of an 18 ns pulse shows a pronounced absorbance around 660 nm, ascribable to the CS state formed by the L conformation (Figure 8). The **Zn$^{+\cdot}$–Au$^{\cdot}$** CS state derived by electron transfer in the L conformation decays with an exponential law characterized by a lifetime of 12 ns (Figure 8 inset). The residual absorbance is due to the triplet ^{3}**Zn–Au$^+$**, which decays with a lifetime of 6.8 μs and has a yield of about 15% of the model **Zn**. The residual triplet yield Φ_T is in agreement with the one calculated from the equation $\Phi_T = 0.4$ ($\Phi_{T0}\ \tau_{^1Zn-Au^+}/\tau_0$), which corresponds to an intersystem crossing reaction from a quenched singlet state and the contribution from only about 40% of the whole population, that is, the L conformation. This implies that the fraction of S conformation, that is, 60%, does not contribute to the triplet formation, as would be expected from a very rapid quenching of the singlet excited state by electron transfer in the compact conformation.

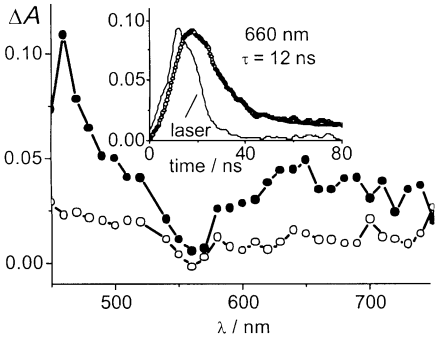

Figure 8. Transient absorption difference detected in oxygen-free acetonitrile solution of **Zn–Au$^+$** measured at 30 ns (●) and 60 ns (○) after an 18 ns laser pulse at 532 nm, 12 mJ. In the inset the absorption decay detected at 660 nm and the relative fitting are reported with the instrumental profile.

Zn–Cu$^+$–Au$^+$: The transient absorption spectra registered at the end of a 35 ps laser pulse for the catenate **Zn–Cu$^+$–Au$^+$** and for the related models **Zn** and **Au$^+$**, are reported in Figure 9. The transient spectrum of the array is essentially

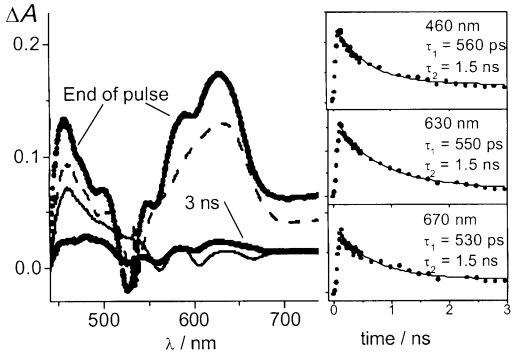

Figure 9. Differential transient absorbances at the end of a 35 ps laser pulse (532 nm; 2.5 mJ) are reported for acetonitrile solutions of: **Au$^+$** (– – –), **Zn** (——), and **Zn–Cu$^+$–Au$^+$** (●); differential transient absorbance measured at 3 ns after laser pulse is reported for **Zn–Cu$^+$–Au$^+$**. The model absorbance was adjusted to have the same number of photons as are absorbed by the same unit in the array. Decays and fittings at selected wavelengths for an acetonitrile solution of **Zn–Cu$^+$–Au$^+$** are reported on the right side.

the superposition of the spectra of the models, without any new spectral features. The kinetic traces taken at three representative wavelengths (460 nm, 630 nm, 670 nm), reported in Figure 9, can be fitted by a bi-exponential decay with lifetimes of 550 ps and 1.5 ns. The shorter lifetime is in perfect agreement with the 540 ps luminescence lifetime (Table 2) and is therefore assigned to ^{1}**Zn–Cu$^+$–Au$^+$**, whereas the longer one is typical of the gold–porphyrin triplet and is assigned to **Zn–Cu$^+$–^{3}Au$^+$**, which is formed by direct excitation of the gold–porphyrin moiety. The measured yield of the latter state is identical to that of the model **Au$^+$**. The residual spectrum at 3 ns in Figure 9 hardly shows any specific absorbance around 670 nm, indicating the absence of a zinc–

porphyrin cation, as confirmed by a nanosecond laser flash photolysis experiment reported in Figure 10. In this figure, the spectra measured in oxygen-free acetonitrile solutions of **Zn–Cu$^+$–Au$^+$** at 25 and 50 ns after an 18 ns laser pulse are

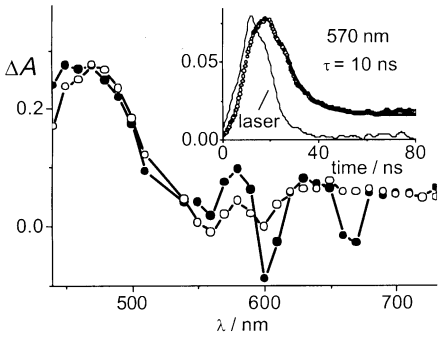

Figure 10. Transient absorption difference detected in an air-free acetonitrile solution of **Zn–Cu$^+$–Au$^+$** measured at 25 ns (●) and 50 ns (○) after an 18 ns laser pulse (532 nm, 13 mJ). In the inset, the transient absorption decay detected at 570 nm and the fitting are reported with the instrumental profile.

shown. The initial spectrum has marked bands at 570 and 450 nm, which decay rapidly with a lifetime of 10 ns (inset of Figure 10), leaving a strong residual absorbance after 50 ns, whose features are consistent with the triplet (λ_{max} = 480 nm) localized on the Zn porphyrin chromophore **^{3}Zn–Cu$^+$–Au$^+$**, and which decays with a τ = 7.2 μs. In contrast with the case of **Zn–Au$^+$,** no pronounced band or fast decay could be detected around 650–670 nm, typical of the zinc-porphyrin cation absorbance. The bands around 570 and 450 nm could in principle be assigned to two intermediate species of the reaction (Figure 4c), either the excited state **Zn–*Cu$^+$–Au$^+$** or the charge-separated state **Zn–Cu^{2+}–Au$^{\cdot}$**, which is characterized by an oxidized metal complex and a reduced gold–porphyrin radical. Whereas the reduced gold–porphyrin radical is known to have bands around 610 and 445 nm,[15] ***Cu$^+$** displays a band at 570 nm but has a bleaching (increase of transmission) at 450 nm.[13] We therefore assign the spectrum with the 10 ns decay to the charge-separated state **Zn–Cu^{2+}–Au$^{\cdot}$**.

The experimental yield of the Zn–porphyrin triplet, ϕ_T = 0.39, can be accounted for nearly completely[16] by a reduced intersystem crossing from a quenched singlet excited state **^{1}Zn–Cu$^+$–Au$^+$**, according to the equation $\phi_T = \phi_{T0}\tau_{Zn-Cu^+-Au^+}/\tau_0$ (see above for the meaning of the symbols). In addition, the yield determined for **^{3}Zn–Cu$^+$–Au$^+$** seems to exclude **Zn–*Cu$^+$–Au$^+$** as the transient species with a 10 ns lifetime. In fact, a calculation of the yield of **^{3}Zn–Cu$^+$–Au$^+$** according to Equations (1) and (2), on the assumption that the 10 ns species is **Zn–*Cu$^+$–Au$^+$** converting quantitatively to **^{3}Zn–Cu$^+$–Au$^+$**, would imply a ϕ_T on the order of 1, which is quite different from the experimental value of 0.39.

The charge-separated state **Zn–Cu^{2+}–Au$^{\cdot}$** is formed following the quenching of the zinc–porphyrin singlet state to **Zn–*Cu$^+$–Au$^+$** and subsequent electron transfer from the excited copper complex to the gold porphyrin. This process is not followed by a charge shift leading to the fully charge-separated state **Zn$^{+\cdot}$–Cu$^+$–Au$^{\cdot}$**, since no trace of the zinc–porphyrin radical absorbance is detected. Such behavior can be understood from the energy scheme reported in Figure 4c. The charge shift reaction that moves an electron from the zinc porphyrin to the copper complex, **Zn–Cu^{2+}–Au$^{\cdot}$**→**Zn$^{+\cdot}$–Cu$^+$–Au$^{\cdot}$**, has no driving force because both the zinc–porphyrin unit and the copper phenanthroline complex have the same oxidation potential (Table 1) and cannot compete with the deactivation process, which leads to the recombination of charges.

Photoinduced processes and comparison with the rotaxanes: From the data discussed and reported in Tables 2 and 3, the energy level scheme of Figure 4 can be completed with the main reaction steps and the related rate constants, k, calculated from Equation (3), in which τ and τ_0 are the lifetimes of the state in the array and in the model, respectively.

$$k = 1/\tau - 1/\tau_0 \quad (3)$$

The main deactivation of the excited porphyrin singlet state in **Zn–Cu$^+$** is an energy transfer to the excited MLCT manifold localized on the copper complex (ΔG^0 = −0.28 eV). This is supported by the spectral changes accompanying the reaction and by the final, quantitative conversion to the **^{3}Zn–Cu$^+$** state. Reductive quenching of the zinc–porphyrin singlet excited state by the copper(I) complex by electron transfer, though thermodynamically feasible (ΔG^0 = −0.05 eV), is not kinetically competitive with the energy-transfer process.

In **Zn–Au$^+$**, the existence of two extreme conformations L (40%) and S (60%) (Scheme 2) has been inferred from the comparison of steady-state and time-resolved luminescence quenching data and has been confirmed by the triplet porphyrin yields. Whereas electron transfer in the S conformation is too fast to be kinetically resolved by our experiments (except the final recombination of the CS state, for which a lifetime of the order of 50 ps is estimated), the processes in the L conformation could be resolved. Electron transfer from the excited singlet zinc porphyrin to the gold porphyrin has a rate of $1.3\times10^9\ s^{-1}$, lower than the rate ($5\times10^9\ s^{-1}$) previously reported for the corresponding reaction in **Zn$_2$–Au$^+$** (Figure 1). This is fully compatible both with the decrease in the driving force (ΔG^0 = −0.74 eV compared with ΔG^0 = −0.9 eV in **Zn$_2$–Au$^+$**) and with the increase in distance between the reacting partners, from 1.9 nm in **Zn$_2$–Au$^+$** to 2.6 nm in the present case. The distance parameter in addition to a more negative value of ΔG^0 for charge recombination (−1.31 eV in the case of **Zn–Au$^+$** in comparison with −1.22 eV in **Zn$_2$–Au$^+$**), also affects this rate, which is slowed down from $2\times10^8\ s^{-1}$ for **Zn$_2$–Au$^+$** to about $9\times10^7\ s^{-1}$ in the present **Zn–Au$^+$**.

For **Zn–Cu$^+$–Au$^+$**, the primary photoinduced step, energy transfer from the singlet excited state localized on the zinc porphyrin to the MLCT manifold localized on the copper complex, is slower ($k = 1.4\times10^9\ s^{-1}$) than the one occurring in **Zn$_2$–Cu$^+$–Au$^+$** ($k = 5\times10^9\ s^{-1}$). This is consistent with the lower driving force for the reaction in **Zn–Cu$^+$–Au$^+$**,

$\Delta G^0 = -0.28$ eV, compared with $\Delta G^0 = -0.35$ eV for **Zn_2–Cu^+–Au^+**, as well as with the larger distance between reacting partners in the present case. What is somewhat surprising is that the energy-transfer rate in **Zn–Cu^+–Au^+** is nearly half that determined for the same step in **Zn–Cu^+**, $2.7 \times 10^9\ s^{-1}$ (Figure 4a), in spite of the similarity of the components involved in the reaction. This could be explained by the perturbation introduced by the second gold–porphyrin substituent in proximity of the copper complex. After the primary energy-transfer step, the **Zn–*Cu^+–Au^+** state, with the excitation localized on the copper complex unit, can transfer an electron to the gold-porphyrin moiety to yield the charge-separated state **Zn–Cu^{2+}–Au$^{\bullet}$**, which is characterized by an oxidized copper complex center and a reduced gold porphyrin (Figure 4c). A similar reaction occurs in the rotaxane **Zn_2–Cu^+–Au^+** and in that case it is followed within the 20 ps resolution by a charge shift, which yields the fully charge-separated state **$Zn_2^{+\bullet}$–Cu^+–Au$^{\bullet}$**. This then recombines to the ground state with a lifetime of 5 ns.[5e] For the rotaxane **Zn_2–Cu^+–Au^+**, the $\Delta G°$ for the charge shift leading to the fully charge-separated state (**Zn_2–Cu^{2+}–Au$^{\bullet}$** → **ZnZn$^{+\bullet}$–Cu^+–Au$^{\bullet}$**) is $\Delta G° = -0.25$ eV. By contrast, the analogous process in the present catenane, corresponding to the hypothetical reaction **Zn–Cu^{2+}–Au$^{\bullet}$** → **Zn$^{+\bullet}$–Cu^+–Au$^{\bullet}$**, has no driving force. The difference between the rotaxane and the catenane is due to changes in the electrochemical properties of both the potential electron acceptor Cu^{II} and the potentially electron-donor zinc–porphyrin unit. In fact, the β-substituted zinc porphyrins of the rotaxane have been replaced by the less powerfully reducing *meso*-substituted zinc porphyrin in the catenane, with oxidation potentials of 0.17 V[5e] and 0.28 V versus Fc^+/Fc for the etio and the tetraryl derivatives, respectively. On the other hand the oxidation of the Cu^I complex unit in **Zn–Cu^+–Au^+**, 0.29 V versus Fc^+/Fc, though higher than the oxidation potential of the model **Cu^+** (Table 1), is considerably lower than the 0.43 V versus Fc^+/Fc measured in **Zn_2–Cu^+–Au^+**.[5e]

In the rotaxane, oxidation of copper(I) to copper(II) occurs at a more positive potential than that of the two zinc–porphyrin units. In other words, it becomes very difficult to oxidize Cu^I, since this complex is directly connected to two powerful electron-withdrawing groups ($Zn^{+\bullet}$ radical cation). By contrast, the oxidation of the central copper(I) complex in the catenane takes place before or simultaneously to that of the zinc porphyrin, providing the Cu^I complex with "normal" redox properties and a much lower oxidation potential than in the rotaxane. The sequence of oxidation processes for both compounds is indicated in Equations (4) (rotaxane) and (5) (catenane) below.

$$\mathbf{Zn_2 - Cu^+ - Au^+} \xrightarrow[+0.18\,V]{-2e^-} \mathbf{Zn^{+\bullet}Zn^{+\bullet} - Cu^+ - Au^+} \xrightarrow[+0.43\,V]{-e^-} \mathbf{Zn^{+\bullet}Zn^{+\bullet} - Cu^{2+} - Au^+} \quad (4)$$

$$\mathbf{Zn - Cu^+ - Au^+} \xrightarrow[+0.29\,V]{-2e^-} \mathbf{Zn^{+\bullet} - Cu^{2+} - Au^+} \quad (5)$$

It may seem paradoxical that in the rotaxane, although the copper complex is directly bound to two etio zinc porphyrins (electron-rich substituents), its redox potential is higher than the central copper complex of the catenane. This high redox potential is simply due to the order of the oxidation processes sequence, as indicated above.

Changes in redox properties of Cu^I bisphenanthroline derivatives have often been discussed in the literature on the basis of a steric argument. This is based on the fact that bulky substituents at the 2 and 9 positions of the ligand increase the oxidation potentials of Cu^I–bisphenanthroline derivatives, characterized by a tetrahedral geometry, because they resist rearrangement to the flatter structure that is more appropriate for a Cu^{II} oxidation state.[17] This effect does not seem to play any role in the present case; in fact, molecular models show that the restriction to planarization is essentially the same in the catenane and the rotaxane, in agreement with the fact that the substituent at the 2 and 9 positions is, in both cases, a phenyl group.

In the catenanes, the increase in the energy level of the fully charge-separated state **$Zn^{+\bullet}$–Cu^+–Au$^{\bullet}$** and the decrease in the energy level of the primary charge-separated state **Zn–Cu^{2+}–Au$^{\bullet}$** thus lead to an essentially isoenergetic situation of the two states. Accordingly, the primary charge-separated state **Zn–Cu^{2+}–Au$^{\bullet}$**, formed by photoinduced electron transfer from the sensitized copper-complex excited state, recombines to the ground state with a rate of $10^8\ s^{-1}$, without proceeding further in charge separation. Notably, in spite of the absence of a further charge separation step, the lifetime of the present charge-separated state is longer than that of the rotaxane **$Zn_2^{+\bullet}$–Cu^+–Au$^{\bullet}$**, in which the charges are separated over the full distance of the array.

Conclusion

We have shown that in the present catenane structure, the electron and energy-transfer steps originating from the excited zinc–porphyrin unit are slower than in the corresponding rotaxanes, while the efficiencies are still remarkable (ca. 75%). A noticeable difference between the rotaxane **Zn_2–Cu^+–Au^+** and the catenane **Zn–Cu^+–Au^+** is that in the latter case, the second electron transfer (charge shift) does not take place. Nonetheless the lifetime of the charge-separated state in the catenane **Zn–Cu^{2+}–Au$^{\bullet}$** is twice as long as that of the fully charge-separated state in the rotaxane **$Zn_2^{+\bullet}$–Cu^+–Au$^{\bullet}$**. An important and general result for the present series is that the lifetimes of the final charge-separated states are increased by a factor of 2–2.5 in all catenanes compared with the corresponding rotaxanes.

Experimental Section

Synthesis: All reactions were performed under an atmosphere of argon, using standard Schlenk techniques. CH_2Cl_2 was distilled from P_2O_5 and DMF (analytical grade) was filtered through a pad of alumina prior to use. Porphyrin **4**,[9] phenanthroline **1**,[5e] macrocycle **Zn**,[9] [**Au**]PF_6,[5e] [2]catenate [**Zn–Cu–Au**]$(PF_6)_2$,[9] and [2]catenane [**Zn–Au**]PF_6[9] were available from previous studies. Macrocycle **2**,[18] [2]catenate [**Cu**]BF_4,[18] and $[Cu(CH_3CN)_4]PF_6$[19] were prepared according to literature procedures. All the compounds used in photophysical investigations were carefully checked and purified by chromatography when necessary. ^{1}H NMR spectra were obtained on a Bruker Avance 400 spectrometer. Chemical

shifts in ppm are referenced downfield from tetramethylsilane. Labels of the protons of [2]catenane **Zn–Cu**$^+$ are provided in Scheme 1. Mass spectral data were obtained on a ZAB-HF (FAB) spectrometer.

[2]catenane [**Zn–Cu**]PF_6 was prepared in a two-steps procedure as previously described for related catenates.[18] The first step consists of the synthesis of the copper(I) precatenate **3**, which is converted in a second step to the desired catenate. The precursors are represented in Scheme 3.

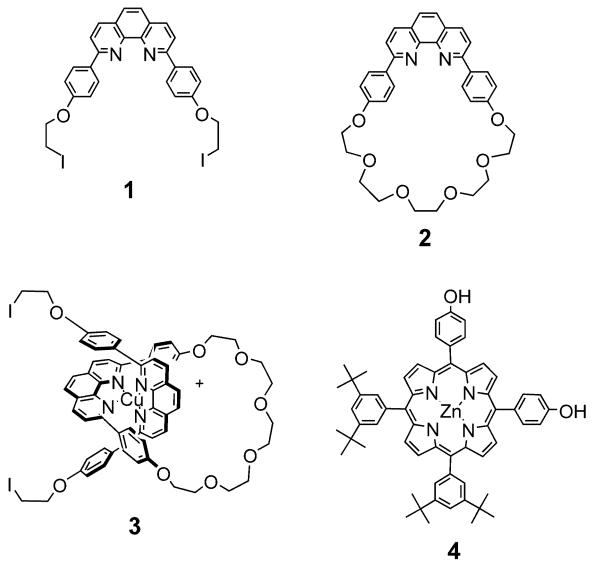

Scheme 3. Precursors for the synthesis of [**Zn–Cu**]PF_6.

Precatenate 3: A degassed solution of $[Cu(CH_3CN)_4]PF_6$ (98.6 mg, 0.265 mmol) in CH_3CN (7 mL) was added by cannula to a pale yellow degassed solution of **1**[5e] (178.1 mg, 0.265 mmol) and **2**[18] (150.6 mg, 0.266 mmol) in CH_2Cl_2 (50 mL). The solution turned dark red immediately. After stirring for 3 h, the solvents were removed in vacuo, leaving a quantitative amount of pure precatenate **3** as a red solid. ^{1}H NMR (300 MHz, CD_2Cl_2): δ = 8.64 (d, ^3J = 8.4 Hz, 2H; $H_{4,7}$), 8.51 (d, ^3J = 8.2 Hz, 2H; $H_{4',7'}$), 8.26 (s, 2H; $H_{5,6}$), 8.08 (s, 2H; $H_{5',6'}$), 7.88 (d, ^3J = 8.2 Hz, 2H; $H_{3,8}$ or $H_{3',8'}$), 7.85 (d, ^3J = 8.2 Hz, 2H; $H_{3,8}$ or $H_{3',8'}$), 7.51 (d, ^3J = 8.6 Hz, 4H; H_o), 7.32 (d, ^3J = 8.6 Hz, 4H; H_o), 6.09 (d, ^3J = 8.6 Hz, 4H; H_m or $H_{m'}$), 6.00 (d, ^3J = 8.6 Hz; H_m or $H_{m'}$), 3.88 (t, ^3J = 6.2 Hz, 4H; H_α), 3.83 (s, 4H; $H_{\varepsilon'}$), 3.88–3.73 (m, 16H; $H_{\alpha',\beta',\gamma',\delta'}$), 3.32 (t, ^3J = 6.2 Hz, 4H; H_β).

[2]catenate [Zn–Cu]PF_6: A degassed solution of precatenate **3** (249.3 mg, 0.172 mmol) and zinc porphyrin **4**[5e] (160.2 mg, 0.1713 mmol) in DMF (16 mL) was added dropwise (1 drop/30 s) to a stirred suspension of Cs_2CO_3 (212 mg, 0.651 mmol) in DMF (32 mL) at 55 °C under argon. After the mixutre had been stirred for 19 h at 55 °C, the solvent was evaporated under reduced pressure. The residue was taken up in CH_2Cl_2 and washed with water. The resulting organic layer was stirred with a 5% aqueous solution of KPF_6 and then separated from the aqueous phase. After evaporation of the solvent, the crude material was purified by repeated column chromatography (SiO_2, CH_2Cl_2/MeOH, 100:0.2) to afford [**Zn–Cu**]PF_6 in 14% yield (52 mg). ^{1}H NMR (400 MHz, CD_2Cl_2): δ = 9.12 (d, ^3J = 4.6 Hz, 2H; H_{py2}), 9.04 (d, ^3J = 4.3 Hz, 2H; H_{py3}), 9.03 (s, 2H; H_{py4}), 8.63 (s, 2H; H_{py1}), 8.63 (d, ^3J = 8.4 Hz, 2H; $H_{4,7}$), 8.42 (d, ^3J = 8.3 Hz, 2H; $H_{4',7'}$), 8.25 (d, ^3J = 8.6 Hz, 4H; $H_{o''}$), 8.14 (s, 2H; $H_{5,6}$), 8.11 (d, ^4J = 1.8 Hz, 4H; H_{op}), 7.84 (d, ^3J = 8.3 Hz, 2H; $H_{3',8'}$), 7.83 (d, ^3J = 8.4 Hz, 2H; $H_{3,8}$), 7.82 (t, ^4J = 1.8 Hz, 2H; H_{pp}), 7.76 (s, 2H; $H_{5',6'}$), 7.48 (d, ^3J = 8.6 Hz, 4H; $H_{m''}$),7.35 (d, ^3J = 8.7 Hz, 4H; H_o), 7.22 (d, ^3J = 8.7 Hz, 4H; $H_{o'}$), 6.28 (d, ^3J = 8.7 Hz, 4H; H_m), 5.99 (d, ^3J = 8.7 Hz, 4H; $H_{m'}$), 4.73 (t, ^3J = 4.1 Hz, 4H; H_β), 4.17 (t, ^3J = 4.2 Hz, 4H; H_α), 3.79 (s, 4H; $H_{\varepsilon'}$), 3.65 (m, 8H; $H_{\alpha'}$ and $H_{\gamma'}$ or $H_{\delta'}$), 3.54 (m, 4H; $H_{\gamma'}$ or $H_{\delta'}$), 3.47 (m, 4H; $H_{\beta'}$), 1.54 (s, 36H; Ht_{Bu}); FAB-MS: *m*/*z*: calcd 1977.7 $[M-PF_6^-]^+$, found 1979.8.

Electrochemistry: A freshly opened bottle of butyronitrile (Acros, > 99%) was used as solvent. Tetra-*n*-butylammonium hexafluorophosphate (puriss) was purchased from Fluka. Cyclic voltammetry experiments were performed on an EG&G Princeton Applied Research Potentiostat/Galvanostat model 273A equipped with an Ifelec IF 3802 recorder. A silver wire served as the reference electrode (Ag/Ag^+). A platinum disk was used as working electrode and a platinum wire as counter-electrode. All of the experiments were conducted under an argon atmosphere in a Metrohm universal recipient, using 5 mL solutions containing 0.1 mol dm^{-3} of supporting electrolyte. Ferrocene (1 mg) was added at the end of each experiment as a potential reference.

Spectroscopic and photophysical measurements: The solvents used were acetonitrile (C. Erba, spectroscopic grade) and butyronitrile (Fluka). Absorption spectra were recorded using a Perkin-Elmer Lambda 9 spectrophotometer and uncorrected emission spectra were detected by a Spex Fluorolog II spectrofluorimeter equipped with a Hamamatsu R-928 photomultiplier tube. Relative luminescence intensities were evaluated from the area (on an energy scale) of the luminescence spectra corrected for the photomultiplier response. The fluorescence quantum yields ϕ_f for the components were obtained with reference to a standard, Zn^{II} 5,10,15,20-tetrakis(3′,5′-di-*tert*-butylphenyl)porphyrin in toluene with ϕ = 0.08.[3f] The phosphorescence spectra of the porphyrin triplets were detected by the same spectrofluorimeter equipped with a phosphorimeter accessory (1934D, Spex). The energies of the electronic levels of the various compounds were derived from emission maxima of the luminescence bands at 77 K.

Fluorescence lifetimes in the 20–2000 ps range were determined by an apparatus based on a Nd:YAG laser (Continuum PY62–10) with a 35 ps pulse at 10 Hz, 532 nm excitation, 1.5 mJ per pulse and a streak camera with 2 ps resolution (Hamamatsu C1587 and M1952). The time profiles were analysed by standard iterative methods. Fluorescence lifetimes longer than 2 ns were detected by an IBH Time-Correlated Single-Photon apparatus with excitation at 337 nm.

Transient absorption spectra in the picosecond time domain were measured by a pump and probe system. The second harmonic (532 nm) of a Nd:YAG laser (Continuum PY62–10) with a 35 ps pulse was used to excite samples with an energy of 2–3 mJ. Optical density of samples at the excitation wavelength was between 0.1 and 0.6. Nanosecond laser flash-photolysis studies were performed by using a Nd:YAG laser (18 ns pulse; 532 nm E = 12–14 mJ) and an Hamamatsu R936 photomultipler tube as detector coupled with a digital oscilloscope. The triplet lifetimes were determined by a laser energy of 0.5 mJ, to prevent second order reactions. The instrumental response was determined from the rise and decay of the $^3Au^+$ signal at 630 nm.

Triplet yields are calculated with respect to the photons absorbed only by the unit of interest in the array and were determined by comparing the transient absorbance in the 600–650 nm region with that of Zn^{II} or Au^{III} 5,10,15,20-tetrakis(3′,5′-di-*tert*-butylphenyl)porphyrin with ϕ_T = 0.72 and 1 for the zinc and the gold porphyrins, respectively.[3j] The yields of ^{3}Zn were determined in the nanosecond experiments at 100 ns delay from the pulse, whereas for $^3Au^+$ it was obtained by the picosecond experiments at the end of the pulse, after correcting for the fast components of the decays and the infinite absorbance.

Experimental uncertainties are estimated to be within 10% for lifetime determination, 20% for quantum yields, 20% for molar absorption coefficients, and 3 nm for emission and absorption peaks, unless otherwise stated. The reported distances were estimated using CPK models.

Acknowledgement

This work was supported by CNR (Italy) and CNRS (France). L.F. acknowledges Ministero dell'Istruzione, dell'Universita' e della Ricerca (FIRB, RBNE019H9K) for support. M.L. thanks the French Ministry of Education, Research and Technology, and N.F. thanks the Japan Scholarship Foundation for fellowships.

[1] a) V. Balzani, F. Scandola, *Supramolecular Photochemistry*, Ellis Horwood, Chichester, **1991**; b) M. R. Wasielewski, *Chem. Rev.* **1992**, *92*, 435–461; c) D. Gust, T. A. Moore, A. L. Moore, *Acc. Chem. Res.* **1993**, *26*, 198–205; d) H. Kurreck, M. Huber, *Angew. Chem.* **1995**, *107*, 992–946; *Angew. Chem. Int. Ed.* **1995**, *34*, 849–866; e) A. Harriman, J.-P. Sauvage, *Chem. Soc. Rev.* **1996**, *25,* 41–48; f) D. Gust, T. A. Moore, A. L. Moore in *Electron Transfer in Chemistry, Volume 3 Part II* (Ed.: V. Balzani), Wiley-VCH, Weinheim **2001**, pp. 272–336.

[2] a) K. Kalyanasundaram, *Photochemistry of Polypyridine and Porphyrin Complexes*, Academic Press, London, **1992**, pp. 369–603; b) *The Porphyrin Handbook* (Eds.: K. M. Kadish, K. M. Smith, R. Guilard), Academic Press, San Diego, **2000**, 10 volume set.

[3] a) G. Kodis, P. L. Lidell, L. de la Garza, P. C. Clausen, J. S. Lindsey, A. L. Moore, T. A. Moore, D. Gust, *J. Phys. Chem.* **2002**, *106*, 2036–2048; b) H. Imahori, D. M. Guldi, K. Tamaki, Y. Yoshida, C. Luo, Y. Sakata, S. Fukuzumi, *J. Am. Chem. Soc.* **2001**, *123*, 6617–6628; c) A. Nakano, A. Osuka, T. Yamazaki, Y. Nishimura, S. Akimoto, I. Yamazaki, A. Itaya, M. Murakami, H. Miyasaka, *Chem. Eur. J.* **2001**, *7*, 3134–3151; d) K. Kilså, J. Kajanus, A. Macpherson, J. Mårtensson, B. Albinsson, *J. Am. Chem. Soc.* **2001**, *123*, 3069–3080; e) D. Holten, D. F. Bocian, J. S. Lindsey, *Acc. Chem. Res.* **2002**, *35*, 57–69; f) I. M. Dixon, J.-P. Collin, J.-P. Sauvage, L. Flamigni, *Inorg. Chem.* **2001**, *40*, 5507–5517; g) M.-S. Choi, T. Aida, T. Yamazaki, I. Yamazaki, *Chem. Eur. J.* **2002**, *8*, 2668–2678; h) L. Flamigni, G. Marconi, I. M. Dixon, J.-P. Collin and J.-P. Sauvage, *J. Phys Chem. B.* **2002**, *106*, 6663–6671; i) T. Kesti, N. Tkachenko, H. Yamada, H. Imahori, S. Fukuzumi, H. Lemmetyinen, *Photochem. Photobiol. Sci.* **2003**, *2*, 251–258; j) A. M. Brun, A. Harriman, V. Heitz, J.-P. Sauvage, *J. Am. Chem. Soc.* **1991**, *113*, 8657–8663; k) J.-H. Ha, J.-S. Cho, D. Kim, J.-C. Lee, T.-Y. Kim, Y. K. Shim, *Chem. Phys. Chem.* **2003**, *4*, 951–958; l) N. Aratani, H. S. Cho, T. K. Ahn, S. Cho, D. Kim, H. Sumi, A. Osuka, *J. Am. Chem. Soc.* **2003**, *125*, 9668–9681.

[4] a) C. J. Chang, J. D. K. Brown, M. C. Y. Chang, E. A. Baker, D. G. Nocera in *Electron Transfer in Chemistry, Volume 3, part II* (Ed.: V. Balzani), Wiley-VCH, Weinheim, **2001**, pp. 409–46; b) M. D. Ward, *Chem. Soc. Rev.* **1997**, *26*, 365–375, and references therein; c) T. Hayashi, H. Ogoshi, *Chem. Soc. Rev.* **1997**, *26*, 365–375, and references therein; d) R. A. Haycock, A. Yartsev, U. Michelsen, V. Sundström, C. A. Hunter *Angew. Chem.* **2000**, *112*, 3762–3765; *Angew. Chem. Int. Ed.* **2000**, *39*, 3616–3619; e) C. A. Hunter, R. K. Hyde, *Angew. Chem.* **1996**, *108*, 2064–2067; *Angew. Chem. Int. Ed. Engl.* **1996**, *35*, 1936–1939; f) F. Felluga, P. Tecilla, L. Hillier, C. A. Hunter, G. Licini, P. Scrimin, *Chem. Commun.* **2000**, 1087–1088; g) Y. Kuroda, K. Sugon, K. Sasaki, *J. Am. Chem. Soc.* **2000**, *122*, 7833–7834; h) A. Prodi, M. T. Indelli, C. J. Kleverlaan, F. Scandola, E. Alessio, T. Gianferrara, L. G. Marzilli, *Chem. Eur. J.* **1999**, *5*, 2668–2679; i) L. Flamigni, M. R. Johnston, L. Giribabu, *Chem. Eur. J.* **2002**, *8*, 3938–3947; j) R. Takahashi, Y. Kobuke, *J. Am. Chem. Soc.* **2003**, *125*, 2372–2373; k) E. Iengo, E. Zangrando, E. Alessio, J.-C. Chambron, V. Heitz, L. Flamigni, J.-P. Sauvage, *Chem. Eur. J.* **2003**, *9*, 5879–5887; l) I.-W. Hwang, H. S. Cho, D. H. Jeong, D. Kim, A. Tsuda, T. Nakamura, A. Osuka, *J. Phys. Chem. B* **2003**, *107*, 9977–9988.

[5] a) J.-C. Chambron, A. Harriman, V. Heitz, J.-P. Sauvage, *J. Am. Chem. Soc.* **1993**, *115*, 6109–6114; b) E. Kaganer, E. Joselevich, I. Willner, Z. Chen, M. J. Gunter, T. P. Jeynes, M. R. Johnston, *J. Phys. Chem. B* **1998**, *102*, 1159–1165; c) G. Hungerford, M. Van der Auweraer, D. B. Amabilino, *J. Porphyrins Phthalocyanines* **2001**, *5*, 633–644; d) L. Flamigni, N. Armaroli, F. Barigelletti, J.-C. Chambron, J.-P. Sauvage, N. Solladie, *New J. Chem.* **1999**, *23*, 1151–1158; e) M. Linke, J.-C. Chambron, V. Heitz, J.-P. Sauvage, S. Encinas, F. Barigelletti, L. Flamigni, *J. Am. Chem. Soc.* **2000**, *122*, 11834–11844; f) M. Andersson, M. Linke, J.-C. Chambron, J. Davidsson, V. Heitz, L. Hammarström, J.-P. Sauvage, *J. Am. Chem. Soc.* **2002**, *124*, 4347–4362; g) N. Watanabe, N. Kihara, Y. Furusho, T. Takata, Y. Araki, O. Ito, *Angew. Chem.* **2003**, *115*, 705–707; *Angew. Chem. Int. Ed.* **2003**, *42*, 681–683; h) L. Flamigni, A. M. Talarico, S. Serroni, F. Puntoriero, M. J. Gunter, M. R. Johnston, T. P. Jeynes, *Chem. Eur. J.* **2003**, *9*, 2649–2659.

[6] a) C. O. Dietrich-Bucheker, J.-P. Sauvage, *Chem. Rev.* **1987**, *87*, 795–910; b) F. Vögtle, T. Dünnwald, T. Schmidt, *Acc. Chem. Res.* **1996**, *29*, 451–460; c) D. B. Amabilino, J. F. Stoddart, *Chem. Rev.* **1995**, *95*, 2725–2828.

[7] a) E. Wasserman, *J. Am. Chem. Soc.* **1960**, *82*, 4433–4434; b) G. Schill, *Catenanes, Rotaxanes and Knots*, Academic Press, New York, **1971**.

[8] a) J. Deisenhofer, H. Michel, *Angew. Chem.* **1989**, *101*, 872–890; *Angew. Chem. Int. Ed. Engl.* **1989**, *28*, 829–847; b) R. Huber, *Angew. Chem.* **1989**, *101*, 849- 870; *Angew. Chem. Int. Ed. Engl.* **1989**, *28*, 848–869; c) W. Kühlbrandt, D. N. Wang, Y. Fujiyoshi, *Nature* **1994**, *367*, 614–621; d) G. McDermott, S. M. Prince, A. A. Freer, A. M. Hawthornthwaite-Lawless, M. Z. Papiz, R. J. Cogdell, N. W. Isaacs, *Nature* **1995**, *374*, 517–521; e) T. Pullerits, V. Sundström, *Acc. Chem. Res.* **1996**, *29*, 381–389.

[9] M. Linke, N. Fujita, J.-C. Chambron, V. Heitz, J.-P. Sauvage, *New J. Chem.* **2001**, *25*, 790–796.

[10] J. Andréasson, G. Kodis, S. Li, A. L. Moore, T. A. Moore, D. Gust, J. Mårtensson, B. Albinsson, *Photochem. Photobiol.* **2002**, *76*, 47–50.

[11] J. R. Kirchhoff Jr. , R. E. Gamache, M. W. Blaskie, A. A. Del Paggio, R. K. Lengel, D. R. McMillin, *Inorg. Chem.* **1983**, *22*, 2380–2384.

[12] I. Carmichael, G. L. Hug in *Handbook of Organic Photochemistry, Vol. 1* (Ed.: J. C. Scaiano), CRC Press, Boca Raton, **1989**, p. 389.

[13] N. Armaroli, M. A. J. Rodgers, P. Ceroni, V. Balzani, C. O. Dietrich-Buchecker, J.-M. Kern, A. Bailal, J.-P. Sauvage, *Chem. Phys. Lett.* **1995**, *241*, 555–558.

[14] See for example references [1b, 3b, 3f, 5a, 5e].

[15] a) Z. Abou-Gamra, A. Harriman, *J. Chem. Soc. Faraday Trans. 2* **1986**, *82*, 2337–2350; b) M. E. Jamin, R. T. Iwamoto, *Inorg. Chim. Acta* **1978**, 27, 135–143.

[16] The exact calculated value is 0.21.

[17] a) M. K. Eggleston, D. R. McMillin, K. S. Koenig, A. J. Pallenberg, *Inorg. Chem.* **1997**, *36*, 172–176; b) M. T. Miller, P. K. Gantzel, T. B. Karpishin, *Angew. Chem.* **1998**, *110*, 1659–1661; *Angew. Chem. Int. Ed.* **1998**, *37*, 1556–1558; c) J. Cody, J. Dennisson, J. Gilmore, D. G. VanDerveer, M. M. Henary, A. Gabrielli, C. D. Sherrill, Y. Zhang, C.-P. Pan, C. Burda, C. J. Fahrni, *Inorg. Chem.* **2003**, *42*, 4918–4929.

[18] C. O. Dietrich-Buchecker, J.-P. Sauvage, *Tetrahedron* **1983**, *24*, 5091–5094.

[19] G. J. Kubas, *Inorg. Synth.* **1990**, *28*, 90–92.

Received: October 23, 2003
Revised: January 12, 2004

Published online: April 15, 2004

